

The Importance of Broad Emission-Line Widths in Single Epoch Black Hole Mass Estimates

R.J. Assef¹, S. Frank^{2,3}, C.J. Grier², C.S. Kochanek^{2,4}, K.D. Denney⁵, B.M. Peterson^{2,4}

ABSTRACT

Estimates of the mass of super-massive black holes (BHs) in distant active galactic nuclei (AGNs) can be obtained efficiently only through single-epoch spectra, using a combination of their broad emission-line widths and continuum luminosities. Yet the reliability and accuracy of the method, and the resulting mass estimates, M_{BH} , remain uncertain. A recent study by Croom using a sample of SDSS, 2QZ and 2SLAQ quasars suggests that line widths contribute little information about the BH mass in these single-epoch estimates and can be replaced by a constant value without significant loss of accuracy. In this Letter, we use a sample of nearby reverberation-mapped AGNs to show that this conclusion is not universally applicable. We use the bulge luminosity (L_{Bulge}) of these local objects to test how well the known $M_{\text{BH}} - L_{\text{Bulge}}$ correlation is recovered when using randomly assigned line widths instead of the measured ones to estimate M_{BH} . We find that line widths provide significant information about M_{BH} , and that for this sample, the line width information is just as significant as that provided by the continuum luminosities. We discuss the effects of observational biases upon the analysis of Croom and suggest that the results can probably be explained as a bias of flux-limited, shallow quasar samples.

Subject headings: galaxies: active — quasars: emission lines

¹NASA Postdoctoral Program Fellow at the Jet Propulsion Laboratory, California Institute of Technology, MS 169-530, 4800 Oak Grove Drive, Pasadena, 91109, USA [email:roberto.j.assef@jpl.nasa.gov]

²Department of Astronomy, The Ohio State University, 140 W. 18th Ave., Columbus, OH 43210, USA

³Observatoire Astronomique de Marseille-Provence, Laboratoire d'Astrophysique de Marseille/LAM, Pôle de l'Étoile Site de Château-Gombert 38, rue Frédéric Joliot-Curie 13388 Marseille, France

⁴The Center for Cosmology and Astroparticle Physics, The Ohio State University, 191 West Woodruff Avenue, Columbus, OH 43210, USA

⁵Marie Curie Fellow at the Dark Cosmology Centre, Niels Bohr Institute, University of Copenhagen, Juliane Maries Vej 30, 2100 Copenhagen, Denmark

1. Introduction

Super-massive black holes (BHs) at the center of galaxies are believed to play a fundamental role in the evolution of galaxies. Accreting BHs, or active galactic nuclei (AGNs), are thought, for example, to be responsible for the quenching of star-formation in galaxies needed to explain the existence of the blue cloud and the red sequence (e.g., Granato et al. 2004; Di Matteo et al. 2005; Hopkins et al. 2005) and for heating gas near the centers of galaxy clusters to stop gas accretion onto the central galaxies (e.g., Croton et al. 2006). This makes characterizing the masses and accretion rates of the BH population across cosmic time crucial to understanding the evolution of galaxies and clusters.

Direct dynamical measurements of the mass of BHs are, however, possible only for nearby quiescent galaxies using spatially resolved velocity measurements inside (or close to) the black hole’s sphere of influence (e.g., Merritt & Ferrarese 2001; Gültekin et al. 2009). Fortunately, AGNs provide a completely different means of directly estimating M_{BH} through reverberation mapping (RM; Blandford & McKee 1982; Peterson 1993). Here it is assumed that the gas responsible for the broad-line emission is virialized and that the broad-line velocity widths are related to the orbital speed of the gas around the black hole. Estimates of M_{BH} are then obtained by combining the width of the emission lines with an estimate of the distance from the BH to the broad line region (R_{BLR}). Since AGNs are typically variable, R_{BLR} is estimated using the time it takes for the broad-emission lines to respond to changes in the accretion disk luminosity.

While the RM technique can in principle be used for sources at any distance, it is time consuming, and has been impractical for luminous and distant objects whose variability timescales are long due to their high luminosity (e.g., Vanden Berk et al. 2004; MacLeod et al. 2010) and time dilation. Local RM observations have, however, shown that R_{BLR} is tightly correlated with the luminosity of the accretion disk (e.g., Kaspi et al. 2000; Bentz et al. 2009b). This allows one to estimate R_{BLR} directly from the luminosity, and hence estimate M_{BH} from the single-epoch (SE) spectra used to determine the line widths. In practice, SE M_{BH} estimates are obtained by means of

$$M_{\text{BH}} = f \frac{(\Delta v)^2 L_{\lambda}^{\alpha}}{G} \quad (1)$$

where Δv is the velocity width of a given broad emission line, L_{λ} is the luminosity of the continuum at an associated wavelength λ (in Å), $\alpha \approx 1/2$ but may depend weakly on λ , G is the gravitational constant and f is a dimensionless factor that accounts for the geometry and inclination of the BLR and the characterization of the line width used in defining the relation. The two most common line-width characterizations are the full-width at half maximum (FWHM) and the line dispersion (σ_l ; see, e.g., Peterson et al. 2004). The most common

combinations of broad lines and continuum luminosities used are $H\beta$ and L_{5100} ($\alpha = 0.519$, Bentz et al. 2009b) at low redshift, and $Mg\ II$ with L_{3000} ($\alpha = 0.47$, McLure & Jarvis 2002) or $C\ IV$ with L_{1350} ($\alpha = 0.53$, Vestergaard & Peterson 2006) at higher redshifts, where these lines appear at observed-frame optical wavelengths.

Recently, Croom (2011, hereafter C11) used a large sample of quasars from the Sloan Digital Sky Survey (SDSS, York et al. 2000), the 2dF QSO Redshift Survey (2QZ, Croom et al. 2004) and the 2dF-SDSS LRG and QSO Survey (2SLAQ, Richards et al. 2005) to study the importance of line-width estimates for the accuracy of SE M_{BH} estimates. For each of the $H\beta$, $Mg\ II$, and $C\ IV$ lines, C11 observed that the distributions of SE M_{BH} estimates were not significantly different before and after scrambling the line widths across the sample. C11 also noted that the distribution of line widths with redshift was relatively narrow and showed little evolution with redshift. C11 concluded that line widths provide little additional information about BH masses as required by equation (1) compared to simply using a constant value.

While this is a very interesting observation, it conflates three possible explanations: i) that the underlying assumptions behind equation (1) are not correct and that Δv truly holds no physical information, ii) that for the typically low S/N spectra used, estimates of Δv are so noisy that their physical information is lost or biased, and iii) that due to a conspiracy between the survey selection function and the evolution of the quasar mass, luminosity and accretion rate distributions, the observed distribution of Δv is narrow and non-evolving with redshift, minimizing the effects of its randomization on M_{BH} . In this Letter, we try to separate these issues. First, in §2, we consider the local, reverberation-mapped sample, where independent indirect estimates of M_{BH} are possible through the well-known correlation with the luminosity of the spheroidal component of the host galaxy. Using this sample, we show that the velocities provide almost as much information on M_{BH} as the luminosities. Then, in §3 we discuss the effects of observational biases on the conclusions of C11. Where needed, we assume a Λ CDM flat cosmology with $H_0 = 73\ \text{km s}^{-1}\ \text{Mpc}^{-1}$, $\Omega_\Lambda = 0.7$ and $\Omega_M = 0.3$.

2. Are Line Widths Important for Accurate BH Mass Estimates?

In order to understand the importance of line widths in SE M_{BH} estimates, we use a sample of 34 nearby AGNs observed in reverberation mapping (RM) campaigns with bulge luminosity measurements at 5100\AA , L_{Bulge} , by Bentz et al. (2009a) using *HST*. Although the target selection is somewhat arbitrary, the sample is approximately volume limited, as luminous, distant sources are generally avoided in RM studies due to cosmological time-dilation

and their intrinsically longer variability timescales. The inherent difficulty in measuring bulge luminosities of distant AGNs further constrains the sample distance. The sample properties are summarized in Table 1.

Every object in our sample has been the subject of at least one RM observational campaign, and many for two or more. For each object we use the mean optical spectrum of each reverberation mapping campaign, and we treat each of the 62 mean spectra as independent objects. While there is typically not enough variability from a single object within an RM campaign to treat each individual spectrum as an independent data point, it is a good approximation to assume each observational campaign provides an independent measurement. Although for any one object the dynamic range in luminosity is limited, Peterson et al. (2004) and Bentz et al. (2010) show that RM M_{BH} estimates of NGC 5548, the most studied source, are consistent between campaigns ($\Delta \log M_{\text{BH}} \approx 0.14$ dex). Table 1 also lists the number of individual spectra used to build each mean spectrum.

The host-corrected AGN continuum luminosities at 5100Å, L_{5100} , are taken from Bentz et al. (2009a), while the broad H β FWHM and σ_l measurements are taken directly from the references listed in Table 1. While this leads to some heterogeneity in the recipes used to make the line-width measurements, the (typically) extremely high S/N of the mean spectra minimizes the resulting systematic errors (Denney et al. 2009a). The distributions of the sample in H β FWHM, continuum L_{5100} , bulge L_{Bulge} , and estimated black hole mass are shown in Figure 1.

The ideal test to determine whether the velocity widths hold information about the BH mass would compare these single-epoch mass estimates to dynamical M_{BH} measurements for the same objects. Unfortunately, few AGNs exist with dynamical measurements of M_{BH} , rendering such a test infeasible at present. Studies of quiescent galaxies, however, have determined that there is a strong correlation between the mass of the central BH and the luminosity of the spheroidal component of its host galaxy (e.g., Marconi & Hunt 2003; Graham 2007, 2012). So while we lack dynamical estimates of M_{BH} for comparison, we can assess the reliability of SE M_{BH} estimates simply by using L_{Bulge} as a proxy and studying how well they hold to the $M_{\text{BH}} - L_{\text{Bulge}}$ correlation.

We estimate SE BH masses for each object by means of equation (1), using the mean continuum luminosity at 5100Å and either the FWHM or the σ_l line width characterization of the mean H β spectrum. We evaluate the correlation strength between M_{BH} and L_{Bulge} using the Spearman rank-order coefficient, r_s , finding a value of $r_s^0 = 0.69$ (0.63) when using the FWHM (σ_l) for the mass estimates. Given the number of data points, the probability of obtaining such a value of r_s^0 in the absence of a correlation is $P_{\text{Ran}} = 7.4 \times 10^{-10}$ (5.4×10^{-8}). As expected, our SE M_{BH} estimates are very well correlated with the luminosity of the

spheroidal component of their host, suggesting these SE estimates can be quite accurate.

The amount of information obtained by using accurate line-width estimates can then be tested by re-estimating r_s using M_{BH} estimates obtained with randomly selected values for the line widths. In practice, we randomly re-distribute the measured line widths across the objects in our sample 500 times, essentially bootstrap resampling the observed FWHM distribution, estimating r_s for each realization. In this procedure we never assign a measurement its true line width, although doing so does not alter our main conclusions. Figure 2 shows the resulting distribution of the r_s coefficients compared to the value obtained before modifying the original line widths, r_s^0 . We only show the results for the FWHM, as those using σ_l are very similar. Note that r_s^0 is significantly above the distribution obtained by randomizing the line widths. If we view the values of r_s as Gaussian random numbers, the true value is 4.3σ from the mean of the random trials. The mean value of $r_s = 0.309$ ($P_{\text{Ran}} = 1.5\%$) in the random trials is 8 orders of magnitude less significant than that obtained using the real FWHM estimates. This demonstrates that line widths provide very significant information about M_{BH} and that accurate line-width estimates are crucial for accurate SE M_{BH} estimates in this sample. This is illustrated in the top-right panel of Figure 2, which shows the spread in BH mass ratio obtained by combining all 500 random realizations. The difference in the estimated M_{BH} is strongly peaked but also with broad wings, with a standard deviation of 0.65 dex. We find similar results if we include each source only once.

Using the same formalism, we can also investigate the importance of the continuum luminosity for SE M_{BH} estimates by randomizing the continuum luminosities rather than the line-width estimates. The resulting r_s distribution is also shown in Figure 2, and it looks very similar to that obtained by randomizing the line widths. This is not surprising, as in our sample the ~ 2 dex dynamic range in $L_{5100}^{1/2}$ is similar to that of FWHM² (see Fig. 1). The mean Spearman Rank-order coefficient of the randomized distributions is $r_s = 0.293$ ($P_{\text{Ran}} = 2.1\%$) so, for this sample, accurate line widths are just as important as accurate luminosities for SE M_{BH} estimates. Finally, as a cross-check, one can also estimate the probability that the $M_{\text{BH}} - L_{\text{Bulge}}$ correlation could randomly arise in our sample. We randomize the sample in both L_{5100} and the FWHM, and, as expected, we find an r_s distribution consistent with no correlation. The mean of the distribution is $r_s = -1.7 \times 10^{-3}$, implying $P_{\text{Ran}} = 99\%$.

3. Discussion

Unless the results of the previous section are not applicable at higher redshift, which is physically implausible, we must now look into the possibility that C11’s results are either

due to the low S/N of the spectra or a conspiracy between the surveys and the shape and evolution of both the QSO luminosity and Eddington ratio distributions that leaves the observed line widths in a nearly redshift independent distribution. We note that the sample of C11 is overwhelmingly dominated by SDSS observations, accounting for 100%, 71% and 86% of the $H\beta$, $Mg\text{ II}$ and $C\text{ IV}$ measurements, respectively. For simplicity, the following discussion focuses solely on the SDSS data.

Denney et al. (2009a) have shown that $H\beta$ line-width estimates can be significantly in error for low signal-to-noise ratio (S/N) spectra, with systematic and random error components that scale with S/N . The errors are small for $S/N \sim 20$, but at a typical $S/N \sim 5$, Denney et al. (2009a) observed a shift of 0.10 dex to larger BH masses, and the dispersion increased by 0.12 dex. While in principle this shift could be due to either errors in the line widths or continuum luminosities, L_{5100} is quite insensitive to S/N and M_{BH} only depends on its square root (eqn. [1]). Thus, the errors in M_{BH} found by Denney et al. (2009a) should be dominated by uncertainties in the line-width measurements induced by poor S/N .

Given these results, we then consider whether the SDSS data are simply too noisy. We investigated this possibility using a stacking analysis of the SDSS QSO spectra. We use $C\text{ IV}$ because it has a clean local continuum, and is the line most affected by systematic issues in low S/N spectra (see, e.g., Assef et al. 2011). While this is not ideal, since our discussion and the results of Denney et al. (2009a) have focused solely on $H\beta$, it is still useful since C11 reached identical conclusions for all three of the main QSO broad emission lines used for M_{BH} estimates ($H\beta$, $Mg\text{ II}$ and $C\text{ IV}$). The details and analysis of these stacked spectra, as well as for $Mg\text{ II}$, are presented by Frank et al. (in prep.). The stacks are produced by averaging approximately 7200 QSO SDSS spectra from the sample of Shen et al. (2008, hereafter S08) in the redshift range $1.857 < z < 3.118$ and in the small absolute magnitude range $-27.6 < M_i < -26.6$ mag, divided into 33 bins of FWHM as measured by S08. SDSS quasar redshifts are determined from all possible absorption and emission lines, minimizing the effects of possible $C\text{ IV}$ blueshifts upon z (see Adelman-McCarthy et al. 2008, for details). In the selection process, known BALQSOs were rejected as they can significantly bias the resulting combined spectra. Before stacking, each individual spectrum is corrected for Galactic reddening using the extinction map of Schlegel et al. (1998), shifted into the rest frame, and normalized by the flux near a rest-frame wavelength of 1700\AA . The resulting spectra are then continuum subtracted and averaged, and the FWHM is measured directly from the stacked spectra. Our results are qualitatively insensitive to whether we use the median or averaged stacked spectra.

Figure 3 compares the FWHM measured from the stacked spectra with the mean and median FWHM estimates of S08 in each bin. We find that the FWHM of the mean spectra

agree with the mean/median of the individual estimates. Note, however, that they are moderately biased, particularly at the high velocity end. These issues are explored further by Frank et al. (in prep.). We have also repeated the process for different bins of M_i , and find qualitatively similar results for all absolute magnitudes. Overall, we consider it is unlikely that the line-width measurements are noisy enough to explain the C11 results, since on average they retain the information of the high S/N stacks, and C IV is the line that is most likely to be affected by systematic biases. Furthermore, we note that C11 uses the inter-percentile value to characterize the line widths for Mg II and C IV, and these should be more robust at lower S/N than the FWHM.

Thus, we are left with the conclusion that the narrow and apparently unevolving distribution of line-width measurements in the C11 sample (see his Fig. 1) are caused by a combination of evolution in the Eddington ratio distribution, the quasar luminosity function (QLF) and the SDSS selection function. For example, Figure 4 shows the distribution of Mg II line widths from S08, selected because they span the broadest range of redshifts. With the simplifying approximation that $\alpha = 1/2$ in equation (1), the line width is given by

$$\Delta v \propto \frac{L^{1/4}}{\ell_{Edd}^{1/2}}, \quad (2)$$

where ℓ_{Edd} is the Eddington ratio. We know from Kollmeier et al. (2006) that the ℓ_{Edd} distribution of broad-line quasars is narrow. For these bright SDSS AGNs, the steep QLF ($dn/dL \propto L^{-3.1}$ for $z < 2.4$, Richards et al. 2006) means that at any given redshift half of quasars are within 0.35 mag of the survey flux limit, corresponding to a velocity spread of only 0.035 dex (8%) if we neglect the narrow width of the ℓ_{Edd} distribution. Thus, at fixed redshift we should expect a narrow velocity distribution.

The distribution of Δv also shows little evolution with redshift. Note that the luminosity of objects at the flux limit evolves as $L_{min} \propto \Gamma(z)^2$, where $\Gamma(z) = D_L(z) (1+z)^{-0.28} \sim z^{1.07}$ for our cosmology and a mean quasar spectral slope of $f_\nu \propto \nu^{-0.44}$ (Vanden Berk et al. 2001). Hence, at fixed ℓ_{Edd} , the apparent evolution of their associated line widths is $\Delta v \propto \Gamma(z)^{1/2} \sim z^{0.54}$. If we compare this “passive” evolution rate to that observed for Mg II (Fig. 4), we find that the differences are already surprisingly small. Taken at face value, the difference between the “passive” evolution model and the observed $\text{FWHM} \propto \Gamma^{0.16}$ implies an evolution in the Eddington ratio of $\ell_{Edd} \propto \Gamma^{0.68} \sim z^{0.73}$. Hence, the slow evolution of Δv may be related to quasar “downsizing” (e.g., Cowie et al. 2003). Whether the slow evolution is due to general changes in the accretion rates with z or evolution in ℓ_{Edd} as a function of M_{BH} is a complex problem beyond the scope of this paper. Recent modeling of the QLF and observed ℓ_{Edd} distributions by Shankar et al. (2011) suggests that ℓ_{Edd} likely evolves in both manners, increasing with increasing z and decreasing M_{BH} . That the net result would be

to leave almost no apparent evolution is then simply a coincidence. Adding the significant noise in the line-width measurements of low S/N spectra may further blur the signs of a weak evolution with redshift. Since line widths are clearly essential for SE M_{BH} estimates in the local reverberation mapped sample, this seems to be the most natural explanation of the C11 result. We conclude that line widths are as important as continuum luminosities for determining accurate BH masses, but that the evolution of the QSO population likely conspires with the survey flux limit to conceal this in shallow surveys such as SDSS.

We thank David H. Weinberg, Daniel K. Stern, Alister Graham and Scott Croom for comments and suggestions that helped improve our work. CSK is supported by NSF grant AST-1004756. BMP and CJK are grateful from support by NSF grant AST-1008882.

REFERENCES

- Adelman-McCarthy, J. K., et al. 2008, *ApJS*, 175, 297
- Assef, R. J., Denney, K. D., Kochanek, C. S., et al. 2011, *ApJ*, 742, 93
- Bentz, M. C., Peterson, B. M., Netzer, H., Pogge, R. W., & Vestergaard, M. 2009a, *ApJ*, 697, 160
- Bentz, M. C., et al. 2007, *ApJ*, 662, 205
- . 2009b, *ApJ*, 705, 199
- . 2010, *ApJ*, 716, 993
- Blandford, R. D., & McKee, C. F. 1982, *ApJ*, 255, 419
- Collin, S., Kawaguchi, T., Peterson, B. M., & Vestergaard, M. 2006, *A&A*, 456, 75
- Cowie, L. L., Barger, A. J., Bautz, M. W., Brandt, W. N., & Garmire, G. P. 2003, *ApJ*, 584, L57
- Croom, S. M. 2011, *ApJ*, 736, 161
- Croom, S. M., Smith, R. J., Boyle, B. J., Shanks, T., Miller, L., Outram, P. J., & Loaring, N. S. 2004, *MNRAS*, 349, 1397
- Croton, D. J., et al. 2006, *MNRAS*, 365, 11

- Denney, K. D., Peterson, B. M., Dietrich, M., Vestergaard, M., & Bentz, M. C. 2009a, *ApJ*, 692, 246
- Denney, K. D., et al. 2006, *ApJ*, 653, 152
- . 2009b, *ApJ*, 702, 1353
- . 2010, *ApJ*, 721, 715
- Di Matteo, T., Springel, V., & Hernquist, L. 2005, *Nature*, 433, 604
- Frank, S., et al. in prep.
- Graham, A. W. 2007, *MNRAS*, 379, 711
- . 2012, *ApJ*, 746, 113
- Granato, G. L., De Zotti, G., Silva, L., Bressan, A., & Danese, L. 2004, *ApJ*, 600, 580
- Grier, C. J., et al. 2008, *ApJ*, 688, 837
- Gültekin, K., et al. 2009, *ApJ*, 698, 198
- Hopkins, P. F., Hernquist, L., Cox, T. J., Di Matteo, T., Martini, P., Robertson, B., & Springel, V. 2005, *ApJ*, 630, 705
- Kaspi, S., Smith, P. S., Netzer, H., Maoz, D., Jannuzi, B. T., & Giveon, U. 2000, *ApJ*, 533, 631
- Kollmeier, J. A., et al. 2006, *ApJ*, 648, 128
- MacLeod, C. L., et al. 2010, *ApJ*, 721, 1014
- Marconi, A., & Hunt, L. K. 2003, *ApJ*, 589, L21
- McLure, R. J., & Jarvis, M. J. 2002, *MNRAS*, 337, 109
- Merritt, D., & Ferrarese, L. 2001, in *Astronomical Society of the Pacific Conference Series*, Vol. 249, *The Central Kiloparsec of Starbursts and AGN: The La Palma Connection*, ed. J. H. Knapen, J. E. Beckman, I. Shlosman, & T. J. Mahoney, 335
- Onken, C. A., & Peterson, B. M. 2002, *ApJ*, 572, 746
- Peterson, B. M. 1993, *PASP*, 105, 247
- Peterson, B. M., et al. 2004, *ApJ*, 613, 682

- Richards, G. T., et al. 2005, MNRAS, 360, 839
- . 2006, AJ, 131, 2766
- Schlegel, D. J., Finkbeiner, D. P., & Davis, M. 1998, ApJ, 500, 525
- Shankar, F., Weinberg, D. H., & Miralda-Escude', J. 2011, ArXiv e-prints
- Shen, Y., Greene, J. E., Strauss, M. A., Richards, G. T., & Schneider, D. P. 2008, ApJ, 680, 169
- Vanden Berk, D. E., et al. 2001, AJ, 122, 549
- . 2004, ApJ, 601, 692
- Vestergaard, M., & Peterson, B. M. 2006, ApJ, 641, 689
- York, D. G., et al. 2000, AJ, 120, 1579

Table 1. Reverberation Mapping Sample

Object	$\log L_{5100\text{\AA}}$ erg s ⁻¹	$\log L_{\text{Bulge}}$ erg s ⁻¹	FWHM km s ⁻¹	σ_l km s ⁻¹	N _{Spec}	Ref.
Mrk335	43.73 ± 0.05	43.14	1792 ± 3	1380 ± 6	123	1
	43.81 ± 0.05	43.14	1679 ± 2	1371 ± 8	25	1
PG0026+129	44.95 ± 0.08	44.36	2544 ± 56	1738 ± 100	53	1
PG0052+251	44.78 ± 0.09	44.12	5008 ± 73	2167 ± 30	56	1
F9	43.94 ± 0.06	44.10	5999 ± 60	2347 ± 16	29	1
Mrk590	43.55 ± 0.05	43.59	2788 ± 29	1942 ± 26	24	1
	43.06 ± 0.06	43.59	3729 ± 426	2168 ± 30	17	1
	43.33 ± 0.05	43.59	2743 ± 79	1967 ± 19	16	1
	43.61 ± 0.08	43.59	2500 ± 43	1880 ± 19	17	1
3C120	44.09 ± 0.09	43.19	2327 ± 48	1249 ± 21	52	1
Akn120	43.95 ± 0.04	44.01	6042 ± 35	1753 ± 6	20	1
	43.61 ± 0.06	44.01	6246 ± 78	1862 ± 13	20	1
Mrk79	43.60 ± 0.06	43.80	5056 ± 85	2314 ± 23	20	1
	43.71 ± 0.06	43.80	4760 ± 31	2281 ± 26	19	1
	43.64 ± 0.06	43.80	4766 ± 71	2312 ± 21	23	1
	43.54 ± 0.05	43.80	4137 ± 37	1939 ± 16	24	1
PG0804+761	44.88 ± 0.09	44.18	3053 ± 38	1434 ± 18	70	1
PG0844+349	44.19 ± 0.06	43.73	2694 ± 58	1505 ± 14	48	1
Mrk110	43.64 ± 0.06	42.65	1543 ± 5	962 ± 15	21	1
	43.72 ± 0.07	42.65	1658 ± 3	953 ± 10	14	1
	43.49 ± 0.15	42.65	1600 ± 39	987 ± 18	28	1
PG0953+414	45.15 ± 0.07	44.56	3071 ± 27	1659 ± 31	35	1
NGC3227	42.86 ± 0.08	43.23	4445 ± 134	1914 ± 71	23	1
	42.32 ± 0.05	43.23	5103 ± 159	2473 ± 26	26	1
	42.11 ± 0.04	43.23	3972 ± 25	1749 ± 4	75	2
NGC3516	43.17 ± 0.15	43.77	5236 ± 12	1584 ± 1	74	2
NGC3783	43.02 ± 0.05	42.86	3770 ± 68	1691 ± 19	73	3
NGC4051	41.88 ± 0.05	42.86	1453 ± 3	1500 ± 34	29	1
	41.82 ± 0.03	42.86	799 ± 2	1045 ± 4	86	4
PG1211+143	44.70 ± 0.08	43.77	2012 ± 37	1487 ± 30	36	1
PG1226+023	45.93 ± 0.07	45.05	3509 ± 36	1778 ± 17	39	1
PG1229+204	43.65 ± 0.06	43.58	3828 ± 54	1608 ± 24	33	1

Table 1—Continued

Object	$\log L_{5100\text{\AA}}$ erg s ⁻¹	$\log L_{\text{Bulge}}$ erg s ⁻¹	FWHM km s ⁻¹	σ_l km s ⁻¹	N _{Spec}	Ref.
NGC4593	42.85 ± 0.04	43.84	5143 ± 16	1790 ± 3	25	5
PG1307+085	44.82 ± 0.06	44.26	5059 ± 133	1963 ± 47	23	1
IC4329A	42.89 ± 0.07	44.36	5964 ± 134	2271 ± 58	25	1
Mrk279	43.66 ± 0.06	43.61	5354 ± 32	1823 ± 11	< 40	1
PG1411+442	44.52 ± 0.05	44.08	2801 ± 43	1774 ± 29	24	1
NGC5548	43.35 ± 0.07	43.93	4674 ± 63	1934 ± 5	132	1
	43.09 ± 0.07	43.93	5418 ± 107	2227 ± 20	94	1
	43.31 ± 0.06	43.93	5236 ± 87	2205 ± 16	65	1
	43.02 ± 0.09	43.93	5986 ± 95	3110 ± 53	83	1
	43.28 ± 0.06	43.93	5930 ± 42	2486 ± 13	142	1
	43.33 ± 0.06	43.93	7378 ± 39	2877 ± 17	128	1
	43.48 ± 0.05	43.93	6946 ± 79	2432 ± 13	78	1
	43.39 ± 0.08	43.93	6623 ± 93	2276 ± 15	144	1
	43.19 ± 0.06	43.93	6298 ± 65	2178 ± 12	95	1
	43.55 ± 0.06	43.93	6177 ± 36	2035 ± 11	119	1
	43.46 ± 0.08	43.93	6247 ± 57	2021 ± 18	86	1
	43.06 ± 0.08	43.93	6240 ± 77	2010 ± 30	37	1
	43.06 ± 0.07	43.93	6478 ± 108	3111 ± 131	45	1
	42.87 ± 0.05	43.93	6396 ± 167	3210 ± 642	28	6
PG1426+015	44.60 ± 0.08	44.26	7113 ± 160	2906 ± 80	20	1
Mrk817	43.75 ± 0.07	42.78	4711 ± 49	1984 ± 8	25	1
	43.63 ± 0.06	42.78	5237 ± 67	2098 ± 13	17	1
	43.63 ± 0.05	42.78	4767 ± 72	2195 ± 16	19	1
PG1613+658	44.73 ± 0.07	44.62	9074 ± 103	3084 ± 33	48	1
PG1617+175	44.36 ± 0.09	44.11	6641 ± 190	2313 ± 69	34	1
PG1700+518	45.56 ± 0.05	44.83	2252 ± 85	3160 ± 93	37	1
3C390.3	43.65 ± 0.08	43.62	12694 ± 13	3744 ± 42	104	1
Mrk509	44.16 ± 0.09	43.98	3015 ± 2	1555 ± 7	194	1
PG2130+099	44.40 ± 0.05	42.94	2853 ± 39	1485 ± 15	21	7
NGC7469	43.30 ± 0.04	44.04	1722 ± 30	1707 ± 20	54	1

Note. — Refs: (1) Peterson et al. (2004) and references therein, (2) Denney et al. (2010), (3) Onken & Peterson (2002), (4) Denney et al. (2009b), (5) Denney et al. (2006), (6) Bentz et al. (2007), (7) Grier et al. (2008). Mean line-widths for the spectra of Peterson et al. (2004) and Onken & Peterson (2002) are presented by Collin et al. (2006).

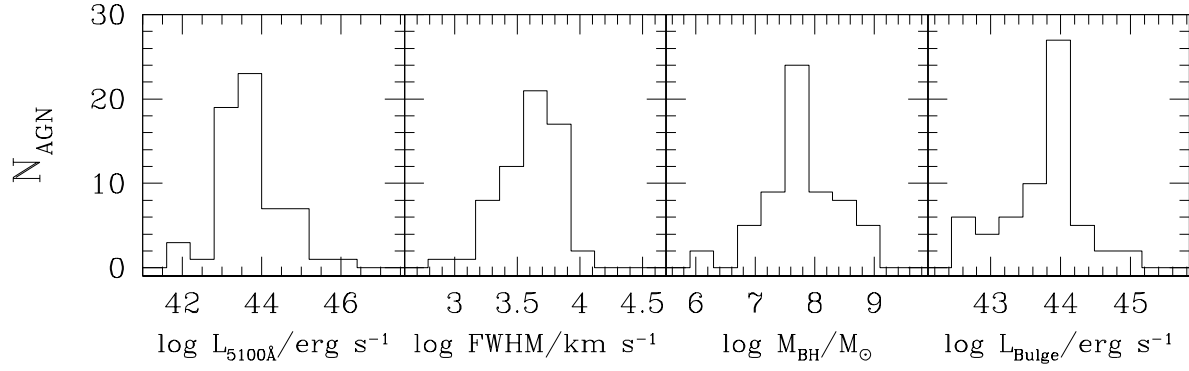


Fig. 1.— Distribution of the physical properties of our sample of nearby AGNs. The panels show the distribution of the L_{5100} AGN continuum luminosities (*left*), broad $\text{H}\beta$ FWHM (*middle left*), SE M_{BH} estimates (*middle right*) and 5100Å bulge luminosities L_{Bulge} (*right*).

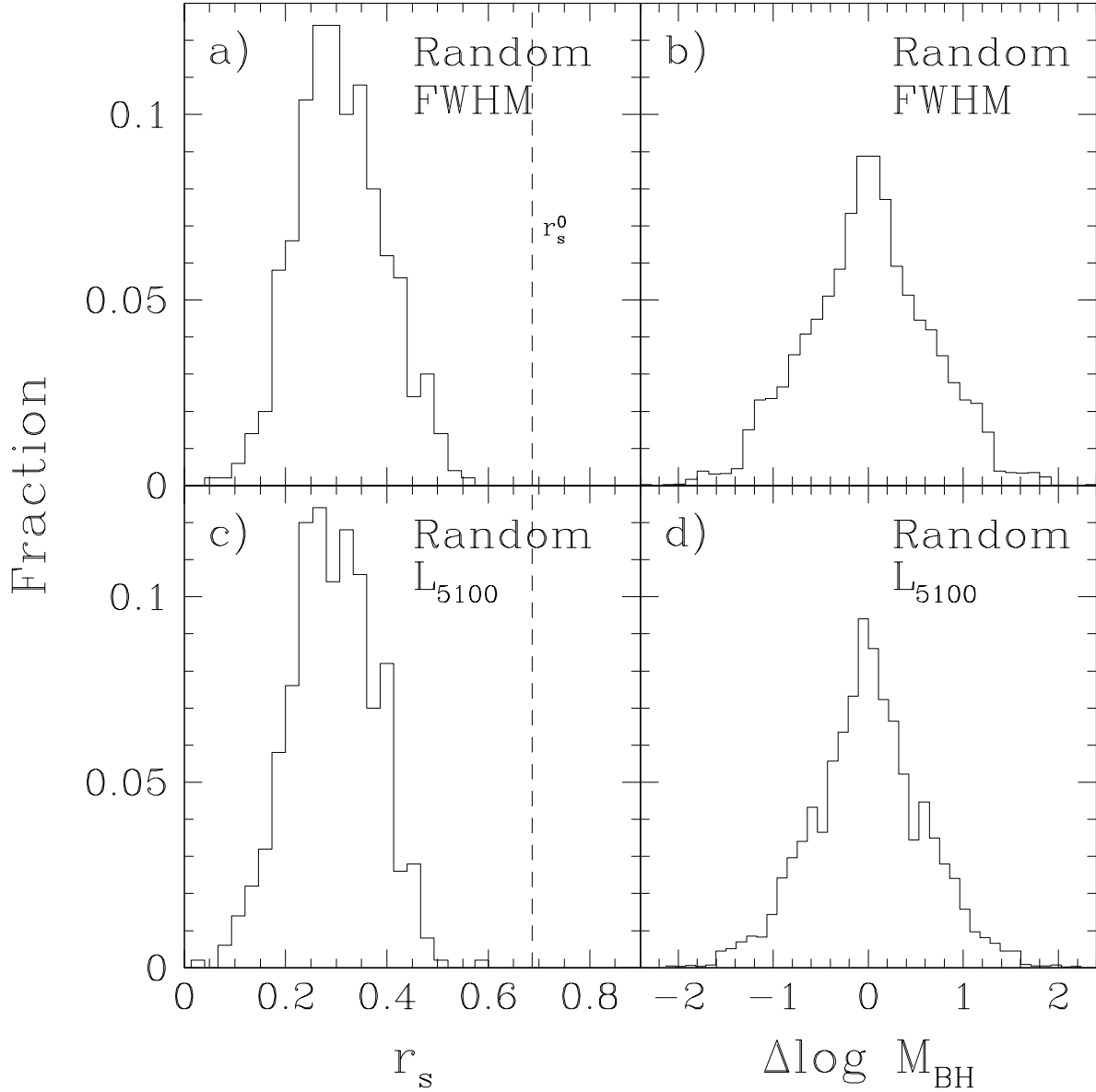


Fig. 2.— Panel *a*) shows the distribution of Spearman rank-order coefficients r_s obtained for 500 randomizations of the FWHM measurements across our sample. The dashed line shows the value obtained using the FWHM measurement that corresponds to each object. Panel *b* shows the distribution of the changes in M_{BH} caused by randomizing the line-widths, i.e., $\Delta \log M_{\text{BH}} = \log M_{\text{BH}}(\text{FWHM}_{\text{Random}}) - \log M_{\text{BH}}(\text{FWHM}_{\text{True}})$. The histogram is constructed by combining the logarithmic change in M_{BH} for every object for every realization. Panels *c*) and *d*) are analogs to panels *a*) and *b*) but after randomizing L_{5100} instead of FWHM.

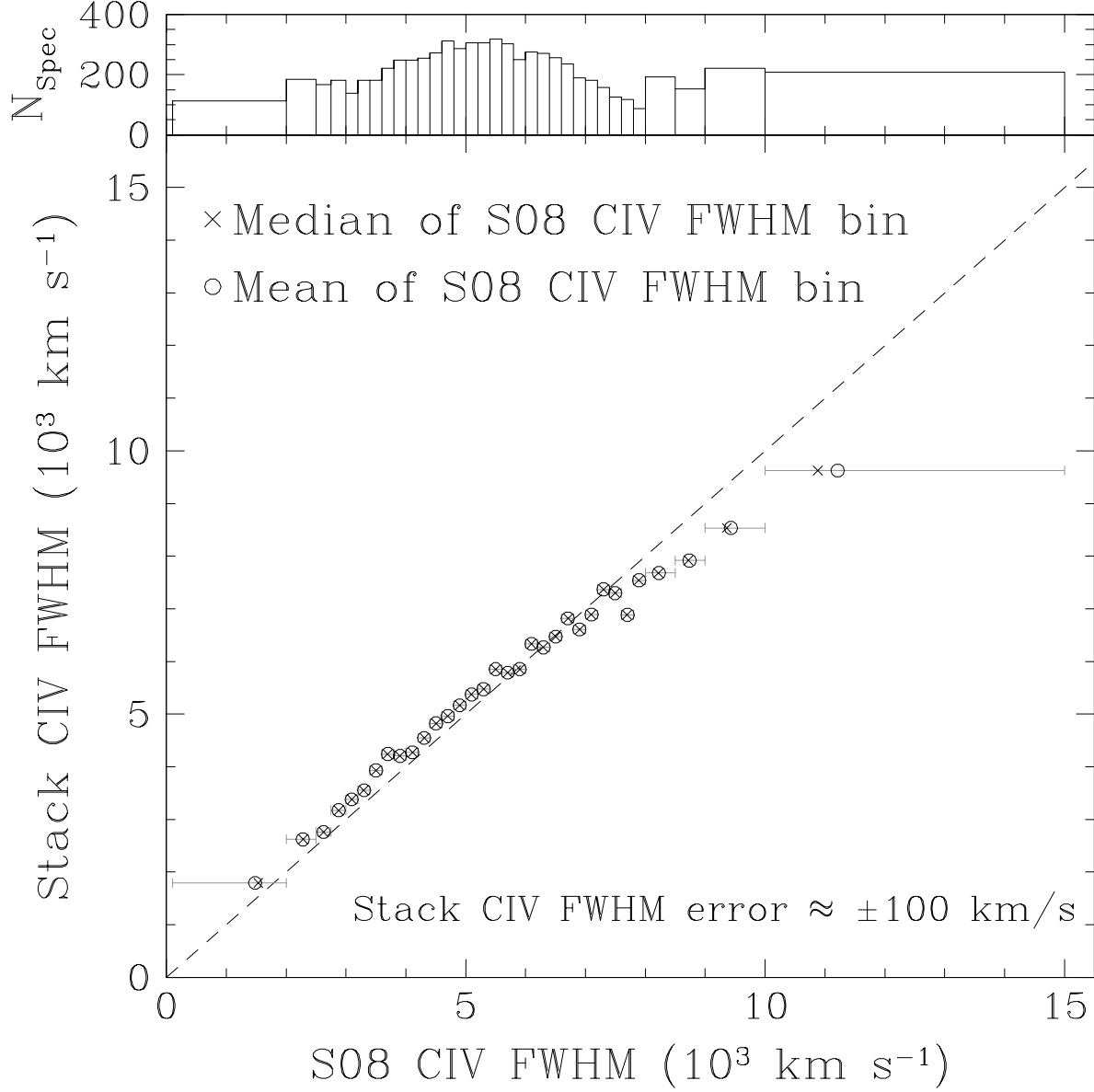


Fig. 3.— The FWHM of the stacked spectra for each bin of individual S08 FWHM estimates. The open circles (crosses) show the mean (median) of the S08 estimates in each bin. The two estimates agree if on the dashed line. The mean and median are generally almost equal. The horizontal error bars span the range of each S08 FWHM bin. The upper panel shows the number of spectra in each S08 FWHM bin.

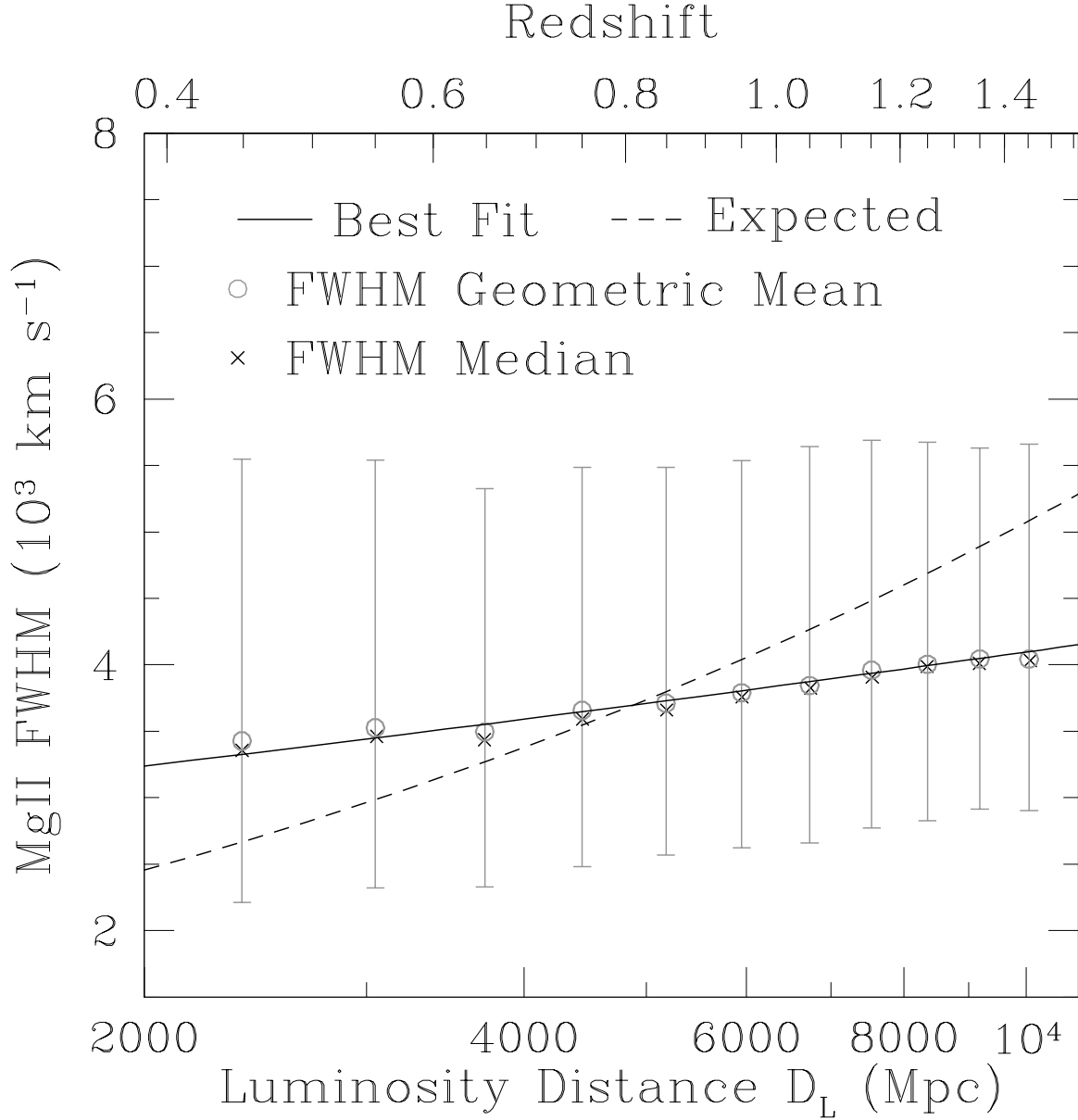


Fig. 4.— The points show the S08 Mg II FWHM as a function of redshift. Gray open circles (crosses) show the FWHM geometric mean (median) of the sample in redshift slices of width $\Delta z = 0.1$ and the error bars enclose 68.3% of objects above and below the mean. The solid black line shows the best-fit evolution of $\text{FWHM} \propto \Gamma(z)^{0.16}$ and the dashed line shows the expected evolution of $\Gamma(z)^{0.5}$ in the absence of ℓ_{Edd} evolution, normalized to the observed trend at $D_L = 5000$ Mpc.